21/12/2012
Final accepted version
Draft Refnº: CHEMISTRY-BIOLOGY-D-12-00356

Blood tolerant laccase by directed evolution

Diana M. Mate[1], David Gonzalez-Perez[1], Magnus Falk[2], Roman Kittl[3], Marcos Pita[1], Antonio L. De Lacey[1], Roland Ludwig[3], Sergey Shleev[2], and Miguel Alcalde[1]

[1]Department of Biocatalysis, Institute of Catalysis, CSIC, 28049 Madrid, Spain.

[2]Biomedical Sciences, Faculty of Health and Society, Malmö University, 20506 Malmö, Sweden.

[3]Food Biotechnology Laboratory, Department of Food Sciences and Technology, University of Natural Resources and Life Sciences, 1190 Vienna, Austria.

*Corresponding author: Miguel Alcalde, Department of Biocatalysis, Institute of Catalysis, CSIC, Cantoblanco, 28049 Madrid, Spain. Phone: +34 915854806, fax: +34 915854760; malcalde@icp.csic.es; malcalde@cheme.caltech.edu.

Running title: blood tolerant laccase

Key words: high-redox potential laccase; halide inhibition; hydroxide inhibition; human blood; bionanodevice; directed evolution.

SUMMARY

High-redox potential laccases are powerful biocatalysts with a wide range of applications in biotechnology. We have converted a thermostable laccase from a white-rot fungus into a blood tolerant laccase. Adapting the fitness of this laccase to the specific composition of human blood (above neutral pH, high chloride concentration) required several generations of directed evolution in a surrogate complex blood medium. Our evolved laccase was tested in both human plasma and blood, displaying catalytic activity whilst retaining a high redox potential at the T1 copper site. Mutations introduced in the second coordination sphere of the T1 site shifted the pH activity profile and drastically reduced the inhibitory effect of chloride. This proof of concept that laccases can be adapted to function in extreme conditions opens an array of opportunities for implantable nanobiodevices, chemical syntheses and detoxification.

INTRODUCTION

The extension of an enzymes' capacity to function in extreme environmental conditions is an issue that promises to deliver countless benefits. Due to their extraordinary versatility, the study of the ligninolytic enzymatic consortium of oxidoreductases secreted by white-rot fungi is of special biotechnological interest -mainly high-redox potential laccases (HRPLs), peroxidases and H_2O_2-supplying enzymes- (Martínez et al., 2009). However, the absence of catalytic activity at neutral/basic pHs, along with the inhibition by modest concentrations of different substances (halides, metal ions, fatty acids, detergents), remain a serious obstacle to their further exploitation. HRPLs (EC 1.10.3.2) that are active under such inclement conditions would be very desirable to be used in applications that range from organic synthesis to bioremediation (Alcalde, 2007; Gianfreda et al., 1999). In addition, HRPLs belong to the exclusive group of oxidoreductases that are capable of accepting electrons directly from the cathode of a biofuel cell or an amperometric biosensor. Indeed, the set of advantages that HRPLs have to offer (*i.e.* high current densities, direct electron transfer, low overpotential for O_2 reduction and high operational stability) situate them among the best suited candidates for enzyme-based bioelectronic devices (Shleev and Ruzgas, 2008). Possibly, one of the most attractive challenges in this field focuses on achieving implantable self-contained wireless 3D-nanobiodevices that work in different physiological fluids (blood, saliva, tears). Such nanobioelectronic devices are comprised of a

biosensor array to detect different metabolites *in vivo* (glucose, insulin), a transmitter/transducer to externalize the information and a biofuel cell to power the entire system. The main shortcomings in the engineering of this type of technology stem from the difficulties in miniaturizing their individual elements (antenna, transducer), and in tailoring reliable and stable enzymes to catalyze the biocathode reaction in which the O_2 dissolved in the fluids is reduced to H_2O (Bullen et al., 2006; Castillo et al., 2004; Kim et al., 2006). Unfortunately, HRPLs are inactive at blood pH (~7.4) and they are also strongly inhibited by chloride concentrations much lower than those found in blood (140-150 mM), which limits this specific application and the use in other areas where basic pHs or chloride ions are presented (*i.e.* dye-stuff proccessing, waste-water treatment, pollutant remediation, pharmaceutical compound synthesis and food proccessing, to name a few (Alcalde, 2007; Gianfreda et al., 1999; Riva, 2006;; Rodgers et al., 2010)).

Here, we report the engineering by directed evolution of the first HRPL that is functional in human blood. The ultimate mutant enzyme obtained through this evolutionary process was characterized comprehensively and its new features were tested on real human blood samples, revealing the mechanisms underlying this unprecedented improvement.

RESULTS AND DISCUSSION

Laboratory evolution approach

Our point of departure in this study was a HRPL (OB-1 mutant) previously tailored in our laboratory by *in vitro* evolution and semi-rational approaches to be active, soluble, highly thermostable and readily secreted by yeast (Maté et al., 2010). To convert OB-1 to an active blood-tolerant laccase, we designed a screening assay based on human blood composition. As real plasma or blood are unsuitable for screening mutant libraries in the experimental context of directed evolution, we developed a surrogate complex medium ("*blood-buffer*") mimicking the biochemical composition of human blood. This buffer contained a laccase colorimetric substrate but it lacked any cells and coagulating agents. Three consecutive rescreens were conducted to rule out the selection of false positives. Like all HRPLs, the OB-1 mutant exhibits neither activity nor significant internal electron transfer at pH 7.4 (Maté et al., 2010). Accordingly, for the first generation the pH of the blood-buffer was set at 6.5, resulting in a decrease in laccase activity of over 90%. In successive generations selective pressure was progressively enhanced until physiological pH values were reached. We took advantage of the high frequency of homologous DNA recombination of the *Saccharomyces cerevisiae* machinery to create diversity (Alcalde, 2010; Gonzalez-Perez et al., 2012). Thus, in each evolution cycle different DNA-recombination methods (both *in vivo* and *in vitro*) were combined to enhance the complexity of the mutant libraries in this pool.

The last round of evolution was dedicated to the detailed rational evaluation of several positions that produced substantial improvements in the total activity by saturation mutagenesis, site directed mutagenesis and mutational recovery (**Figure 1, Table S1 and Supplementary Results Section**). When the last variant of the evolutionary pathway was obtained (ChU-B mutant), it exhibited an increase in total activity in blood-buffer over 40,000-fold *vs* the parental type.

Laccase mutant in blood

The behavior of the mutant laccase was tested in human plasma and blood. Oxygen consumption in physiological fluids enriched with ascorbic acid (a poor laccase substrate naturally present in blood) was monitored with a Clark electrode, revealing comparable responses for plasma and blood (185 and 127 min^{-1}, respectively, **Figure 2a**). The 1.5-fold increase in ChU-B activity in plasma suggested that blood cells interfere with the detection method. To confirm that the enzyme was active under physiological conditions regardless of the reducing substrate used, oxygen reduction against common laccase substrates (ABTS, $K_4[Fe(CN)_6]$) was measured in blood-buffer, obtaining similar values for all compounds tested (**Figure 2a**).

Laccases contain four catalytic copper ions arranged at two different sites: the T1 site, at which the substrate is oxidized; and a trinuclear copper cluster (with one Cu T2 and two Cu T3), at which

oxygen is reduced to water (Morozova et al., 2007). If the laccase is properly connected to an electrode via the T1 Cu, the electroactive surface of the device can replace the electron-donating natural substrates of the enzyme. Redox titration of the T1 Cu site was performed at physiological pH using a micro-spectroelectrochemical cell with a gold capillary electrode (**Figure 2b**). The ChU-B mutant exhibited a high redox potential (+720 mV *vs* NHE) at pH 7.4, and it reversibly cycled between its fully oxidized and fully reduced state. To further verify that the mutant was electrochemically active under physiological conditions, ChU-B was adsorbed onto low-density graphite electrodes and the electrocatalytic response of O_2 reduction by direct electron transfer was recorded at pH 7.4 (**Figure 2c**). No responses were detected for any of the HRPLs tested at this pH.

Inhibition by halides and hydroxides

The novel properties of ChU-B were dissected in terms of its activity *vs* pH and halide inhibition. The pH activity profiles against phenolic (2,6-dimethoxyphenol, DMP) and non-phenolic (2,2'-azino-bis(3-ethylbenzothiazoline-6-sulphonic acid), ABTS) compounds revealed a notable shift towards less acidic values, including a change in DMP optimum activity pH from 4.0 to 5.0-6.0 (**Figure 3a, b**; **Figure S1a, 1b**). At pH 7.0, ChU-B retained ~50% and ~20% of its activity for DMP and ABTS respectively, whereas the parental type displayed negligible activity under these conditions. Similarly, ChU-B activity at pH 6.0 was over 90% and 50% for DMP and ABTS respectively, while

that of the parental type was ~20%. This drastic improvement in activity at near neutral pH led to a small but noticeable increase in ChU-B activity even at pH 8.0. This represents the first HRPL to exhibit activity at neutral/alkaline pH values. To date, the engineering of chimeric laccases had only succeeded in slightly shifting the pH profile, at the expense of sacrificing redox potential (Cusano et al., 2009).

It is well known that increases in pH inhibit laccase activity, due to a decrease in H^+ availability and the binding of OH^- ions to the T2 Cu, which in our laccase is tricoordinated with His64, His397 and one H_2O molecule (Matera et al., 2008; Xu, 1997). HRPLs are also inhibited by halides (fluoride, chloride and bromide, but not iodide), with an inhibitory potency inversely proportional to the diameter of the anion (F^- >Cl^->Br^-). This dependence is possibly due to an access limitation for the binding of the larger halide ions to the laccase catalytic sites (Xu, 1996; Xu, 1997). The I_{50} measured for the different halides (the concentration of halide at which the enzyme retains 50% of its initial activity) was independent of the substrate employed (**Table S2**). The I_{50} of ChU-B for Cl^- improved from 176 to 1025 mM with ABTS as substrate (**Figure 3c**), to the best of our knowledge the highest I_{50Cl^-} reported for any basidiomycete HRPL. It was not possible to measure Br^- inhibition for Chu-B, as the I_{50} of the parental type was already above 1300 mM, impeding measurement by surpassing the limit of substrate solubility at such high salt-concentrations. As expected, there was strong inhibition in the presence of F^- (in the μM range), and

although F^- inhibition was not a goal of the directed evolution study, the I_{50F^-} was slightly enhanced (from 70 to 109 μM, **Figure 3d**). Halide inhibition was also measured at physiological pH values and ChU-B was not sensitive to increasing concentrations of chloride (ranging from 100 to 800 mM) (**Figure 3e**). At pH 7.4, very little H_2O dissociation was observed, although the resulting 251 nM of OH^- may be enough to efficiently bind at the T2 Cu site and promote the inhibition of native HRPLs. The gradual increase in blood-buffer pH throughout evolution reflects the $[OH^-]$ increase and $[H^+]$ decrease, and it permitted a selection of variants that are more tolerant to both hydroxyl and chloride ions in the same screening assay. Comparing ChU-B with other HRPLs revealed that, depending on the substrate, our variant was 12 to 20-fold less sensitive to F^- than the HRPLs from *Trametes trogii* and *Trametes villosa* (Garzillo et al., 1998; Xu, 1996). Similarly, the I_{50Cl^-} of ChU-B was 26 to 164-fold higher than corresponding HRPLs. The ascomycete laccase from *Botrytis aclada* exhibited the highest I_{50Cl^-} described to date (1.4 M with DMP as substrate) (Kittl et al., 2012), yet its negligible activity at neutral pH and poor stability precludes its use in implantable biocathodes or other environmental processes. Comparing ChU-B with laccases from bacterial sources revealed a 1.5-fold better chloride tolerance than that of the halide-resistant polyphenol oxidase from *Marinomonas mediterranea* (Jimenez-Juarez et al., 2005). This halide tolerance of the Chu-B mutant is remarkable given that, as a rule, fungal laccases are much more sensitive to halide

inhibition than low-redox potential laccases from bacteria (Niladevi et al., 2008; Singh et al., 2011).

We assessed maximum turnover rates of ChU-B in blood-buffer. The synergic effect that improved activity at physiological pH in association with a strong chloride tolerance resulted in initial rates of 427 and 143 mol substrate/min/mol enzyme for DMP and ABTS, respectively. In equivalent conditions, the parental type showed almost no activity. Significantly, the turnover rates of the ChU-B mutant was 3 to 4-fold lower than that of the parental type under optimal conditions (*i.e.,* acidic pH and in the absence of inhibitors, **Table S3**). Intrigued by these results, we analyzed mutations in the laccase structure.

Structural analysis of mutations

The laccase catalytic scaffold is formed by the T1 Cu site close to the surface, although the copper is not solvent-exposed. The T1 Cu is trigonally coordinated by His455, His394 and Cys450, the latter forming part of the highly-conserved His451-Cys450-His449 tripeptide, which connects to the trinuclear cluster located 12 Å away. The electrons from T1 Cu are transferred through two intramolecular electron transfer pathways governed by the aforementioned tripeptide to the T2/T3 trinuclear Cu cluster, where O_2 binds and is reduced to two molecules of H_2O. This second active site is buried deep in the laccase structure, with a T2 Cu tricoordinated by two His residues, one molecule of water and two tetracoordinated T3 coppers. The entrance of O_2 and the exit of H_2O to the T2/T3 site occur via two solvent channels.

Bearing in mind that halide/OH^- inhibition allegedly occurs at the T2/T3 cluster, interrupting the internal electron transfer (Naki and Varfolomeev, 1981; Naqui and Varfolomeev, 1980), we expected to find mutations located in the surroundings of the trinuclear copper cluster, or in either of the two channels for oxygen and water transit (Matera et al., 2008; Xu et al., 1998). However, the two mutations introduced in the mature ChU-B (F396I and F454E) were located at the second coordination sphere of the T1 Cu site (**Figure 4**). Indeed, most of the mutations discovered during the course of evolution were placed in the same region (at an average distance of 7.5 Å from the T1 Cu site), indicating an important influence of this region on halide/OH^- inhibition (**Figure S2**, **Table S4**).

F396I was discovered in the first generation and it provoked the greatest improvement in activity of the entire evolutionary process (157-fold increase in activity over the parental type). Additional saturation mutagenesis at this position did not confer any further improvement (**Figure 1**). The highly conserved Phe396 plays a key role in the redox potential of the T1 site, and hence in HRPL catalysis (Matera et al., 2008). Phe396 acts as a bridge connecting the T1 Cu and T2/T3 Cu cluster via Pro395 (contiguous to the coordinating His394 of the T1 Cu) and His397, which coordinates the T2 Cu (**Figure 4**). The F454E mutation was generated by subjecting position 454 to saturation mutagenesis and subsequent screening, as some mutants discovered in the 1st and 3rd generations already contained a mutation at this position

(**Figure 1**, **Figure S3**). We selected six different mutants with F454P/T/A/G/R/E substitutions, which boosted activity in blood-buffer up to 2.5-fold (**Supplementary Results Section**). The F454E mutation is contiguous to the coordinating His455 of the T1 Cu. Analysis of our model revealed that upon mutation, a new H-bond with the imidazole group of His455 appears to be established (**Figure 4**). It is generally accepted that electron transfer from the substrate to the T1 Cu is the rate-limiting step of laccase catalysis (Alcalde, 2007; Gianfreda et al., 1999). Modification of the second coordination sphere of the T1 Cu reduces activity at acidic pH values and simultaneously compensates for T2 Cu inhibition so that ChU-B maintains activity in the presence of halides and OH^-. These results are consistent with previous studies of an ascomycete low-redox potential laccase subjected to comprehensive site-directed mutagenesis at the T1 region (Xu et al., 1998). Recently, the parental type of the current research -the HRPL OB-1 mutant evolved for secretion and stability in yeast, (Maté et al. 2010)- was analyzed by a computational algorithm to understand the physical forces that rule the stability of the variant (Christensen and Kepp, 2012). Indeed, the combination of *in silico* computational methods (based on Montecarlo simulations and molecular dynamics) may provide a new twist in the study of this blood tolerant laccase. In particular, the use of quantum mechanics/molecular mechanics (QM/MM) methods -for mapping internal electron transfer pathways (Guallar et al. 2008)- as well as the protein energy landscape

exploration (PELE) -for assessing the traffic of halides and hydroxides through the laccase structure (Borrelli et al. 2005)- could be valuable approaches to discern the hidden physicochemical principles behind the laccase improvements.

SIGNIFICANCE

HRPLs are considered by many as the green biocatalysts of the 21st century: they easily oxidize hundreds of compounds using oxygen from air and release water as the only by-product (Maté et al., 2011). Moreover, they can be immobilized onto electrodes and they mediate direct electron transfer, permitting their integration into nanobioelectronic devices. Our blood-tolerant laccase displays all these properties, thereby enabling its incorporation into physiological fluids. We are currently designing a full wireless 3D-nanobiodevice prototype for use in human blood, containing an *ad-hoc* transmitter and a biosensor powered by a biofuel cell, to which ChU-B is attached (unpublished material). This technology should permit less invasive and more reliable real-time in-situ monitoring. Indeed, nanobiodevices can minimize the often-critical time to detect a potentially life threatening physiological imbalance and shorten the intervention time for medical teams. With an extraordinary resistance to halides and significant activity at neutral/alkaline pH values, the benefits of our evolved HRPL may also be extended to applications such as the development of medical bioassays, bioremediation (*e.g.* oxidation of pesticides,

PAHs, contained-waste waters, dye processing), pulp-kraft biobleaching, organic syntheses and cofactor/coenzyme regeneration, among other processes in which high pH and/or strong salt contents represent major hurdles (Alcalde et al., 2006; Couto and Herrera, 2006; Kunamneni et al., 2008; Riva, 2006;Witayakran and Ragauskas, 2009).

EXPERIMENTAL PROCEDURES

All chemical reagents were of the highest purity commercially available. The oligonucleotides used along the evolutionary process (**Table S5**) were purchased from Isogen Life Science (De Meern, The Netherlands). Culture media were prepared as described previously (Maté et al., 2010).

Laboratory evolution

For each generation, PCR fragments were cleaned, concentrated and loaded onto a low melting point preparative agarose gel (Bio-Rad, Hercules, CA), and then purified using the Zymoclean gel DNA recovery kit (Zymo Research, Orange, CA). PCR products were cloned under the control of GAL1 promoter of the pJRoC30 expression shuttle vector (kindly donated by Prof. F.H. Arnold from Caltech, CA), replacing the parent gene in pJRoC30. To remove the parent gene, the pJRoC30 plasmid was linearized with *Bam*HI and *Xho*I (New England Biolabs, Hertfordshire, UK), and the linear plasmid was concentrated and purified as described above for the PCR fragments.

First generation: IvAM Using the OB-1 mutant as the parental type (Maté et al., 2010), a library of over 3,000 clones was constructed by *I*n *v*ivo *A*ssembly of *M*utant libraries with different mutational spectra (IvAM) (Zumárraga et al., 2008). Independent mutagenic PCR reactions with *Taq*/$MnCl_2$ (Sigma-Aldrich, Madrid, Spain) and Mutazyme II DNA polymerase (Genemorph II Random mutagenesis kit, Stratagene, CA, USA) were carried out on a gradient thermocycler (Mycycler, Bio-Rad) using the following parameters: 95ºC for 2 min (1 cycle); 94ºC for 0.75 min, 53ºC for 0.75 min, 74ºC for 3 min (28 cycles); 74ºC for 10 min (1 cycle). In a final volume of 50 µL, the *Taq*/$MnCl_2$ PCR amplification contained 90 nM RMLN, 90 nM RMLC, 0.1 ng/µL template, 0.3 mM dNTPs (0.075 mM each), 3% DMSO, 1.5 mM $MgCl_2$, 0.01 mM $MnCl_2$ and 0.05 U/µL *Taq* polymerase. Mutazyme II amplification was carried out with 372 nM RMLN, 372 nM RMLC, 40 ng/µL template, 0.8 mM dNTPs (0.2 mM each), 3% DMSO and 0.05 U/µL Mutazyme II per 50 µL of reaction product. Under these conditions the mutational rates of *Taq*/$MnCl_2$ and Mutazyme II libraries were 0-3 and 4.5-9 mutations per 1,000 bp, respectively. To promote *in vivo* ligation, overhangs of 40 and 66 bp homologous to the linear vector were designed. The two libraries were mixed in equimolar amounts and transformed into competent *S. cerevisiae* cells of the protease-deficient strain BJ5465 (LGC Promochem, Barcelona, Spain) using the yeast transformation kit (Sigma-Aldrich, Madrid, Spain) together with the linearized vector (ratio vector:library 1:4). Transformed cells were plated in SC drop-out plates

and incubated for 3 days at 30ºC. Then, colonies were picked and subjected to the screening assay and to three successive re-screenings, as describes below.

Second generation: Error prone PCR + IvAM Using the 35H10 mutant from the first generation as the parental type, three mutant libraries (~700 clones each) were constructed and independently screened. The first library was prepared with *Taq*/$MnCl_2$, the second with Mutazyme II and the third with IvAM, as described for the first generation.

Third generation: Mutagenic StEP and *in vivo* DNA shuffling Two independent libraries were created and explored using the two best mutants from the second round, 2E3 and 20F1, as the parental types. For the first library, the parental types were independently prepared with to *Taq*/$MnCl_2$ and the mutagenic products *in vivo* shuffled in *S. cerevisiae*. The second library was prepared by *in vitro* recombination through *St*aggered *E*xtension *P*rocess (StEP) (Zhao et al., 1998). The StEP-PCR reaction (50 µL final volume) contained 0.5 µM RMLN, 0.5 µM RMLC, 0.1 ng/µL of each DNA-template, 0.8 mM dNTPs (0.2 mM each), 3% DMSO, 1 mM $MgCl_2$, 0.01 mM $MnCl_2$ and 0.02 U/µL iProof high-fidelity DNA polymerase (Bio-Rad). The PCR conditions were as follows: 95ºC for 2 min (1 cycle); 94ºC for 0.5 min, 55ºC for 0.33 min (90 cycles). An electrophoretic band of ~2 kb was purified and further subjected to mutagenic PCR with Mutazyme II. This mutagenic product was *in vivo* shuffled as described above.

Fourth generation: site-directed and saturation mutagenesis studies

Two individual mutants and three saturation mutagenesis libraries were constructed by *I*n *V*ivo *O*verlap *E*xtension (IVOE) (Alcalde, 2010) using the 27C7 mutant as the parental template. The PCR reactions were carried out using the iProof high-fidelity DNA polymerase.

D205N mutant: The primers for PCR 1 were RMLN and D205N-REV and for PCR 2 were D205N-FOR and RMLC.

N426D mutant: The primers for PCR 1 were RMLN and N426D-REV and for PCR 2 were N426-FOR and RMLC.

Saturation mutagenesis at position 389: The primers for PCR 1 were RMLN and SAT389-REV and for PCR 2 were SAT389-FOR and RMLC.

Saturation mutagenesis at position 396: The primers for PCR 1 were RMLN and SAT396-REV and for PCR 2 were SAT396-FOR and RMLC.

Saturation mutagenesis at position 454: The primers for PCR 1 were RMLN and SAT454-REV and for PCR 2 were SAT454-FOR and RMLC.

Screening assay and high-throughput protocol

Laccase mutant libraries were screened in a medium (blood-buffer) containing the colorimetric laccase substrate ABTS and that simulates the composition of human blood, although it lacks coagulating agents and cells. Blood-buffer composition: 150 mM NaCl, 18 mM $NaHCO_3$, 1 mg/mL glucose, 4.3 mM urea, 0.87 mM $MgSO_4$, 0.4 mM fructose, 0.1 mM L-cysteine and 4.29 mM ABTS in 100 mM sodium phosphate buffer. The blood-buffer pH was set at 6.5 for the first generation and was gradually increased throughout evolution to reach

physiological pH (7.4) in generation 4. The general HTP-screening protocol was as reported previously (Maté et al., 2010) with some modifications. Individual clones were picked and cultured in 96-well plates (Greiner Bio-One, Frickenhausen, Germany) containing 50 μL of minimal medium per well. In each plate, column number 6 was inoculated with the parental type and one well (H1-control) was left uninoculated. Plates were sealed to prevent evaporation and incubated at 30ºC and 80% relative humidity on a shaker at 225 rpm (Minitron-INFORS, Biogen, Spain). After 48 h, 160 μL of expression medium was added to each well and the plates were incubated for 24 h. The plates (master plates) were then centrifuged (Eppendorf 5810R centrifuge, Germany) for 5 min at 3000 x *g* at 4ºC and 60 μL of the supernatant was transferred from the master plate onto a replica plate with the help of a robot (Liquid Handler Quadra 96-320, Tomtec, Hamden, CT). The replica plate was filled with 140 μL of blood-buffer, and after briefly stirring the plates and allowing substrate oxidation in blood-buffer, absorption was measured at 418 nm ($\varepsilon_{ABTS^{\bullet+}}$=36,000 M^{-1} cm^{-1}) in a plate reader (SpectraMax Plus384, Molecular Devices, Sunnyvale, CA). The plates were incubated at room temperature until a green color developed and the absorption was measured again. Relative activities were calculated as the difference between absorption before and after incubation, and normalized against the parental type used as reference in the corresponding plate (the reference parental types were as follows: 1G, OB-1; 2G, 35H10; 3G, 2E3; 4G, 27C7). To rule out false positives,

two consecutive re-screenings were carried out according to our previously described protocol (Maté et al., 2010), but using the blood-buffer assay described above. A third re-screening was introduced to obtain a breakdown of the improvements detected in terms of pH activity profile, Cl^- tolerance and thermostability.

Laccase production and purification

Laccase variants were produced in *S. cerevisiae* (with secretion levels of 8 mg/L) and purified to homogeneity as described previously (Maté et al., 2010). For spectroelectrochemical studies, mutants were over-produced in *Pichia pastoris* after cloning them into the pPICZαA vector under the control of the methanol-inducible AOX1 promoter (*Pichia* expression kit, Life Technologies, Carlsbad, CA). Secretions levels of 43 mg/L were achieved in a 20L autoclavable stainless steel bioreactor (Applikon Biotechnology, Schiedam, The Netherlands).

Measurement of laccase activity in human plasma and blood

Human blood was collected in BD Vacutainer® blood collection tubes (Plymoth, UK). Blood samples were centrifuged for 10 min at 3000 rpm to obtain human plasma, discarding the pellet after having carefully extracted the supernatant. Both plasma and blood were supplemented with 10 mM ascorbic acid as substrate and the pH adjusted to 7.4. The activity of the ChU-B mutant in both physiological fluids was determined by measuring oxygen consumption in solution with a Clark electrode. These experiments were performed using the Oxygraph system (Hansatech Instruments, King´s Lynn, UK), taking

into account the stoichiometry of the reaction: one molecule of O_2 is reduced by oxidizing four substrate molecules. The activity of the ChU-B mutant was further measured in blood-buffer using the same protocol described above and the following substrates: potassium ferrocyanide, $K_4[Fe(CN)_6]$ (5 mM final concentration); ABTS (5 mM final concentration); and ascorbic acid (10 mM final concentration).

Biochemical characterization

Determination of maximum turnover rates in blood-buffer: The initial turnover rates were determined in blood-buffer (pH 7.4) for ABTS and DMP. A typical reaction started upon the addition of the enzyme (4.7 and 22.7 nM for ABTS and DMP, respectively) to the assay mixture (1.3 mM ABTS or 2.8 mM DMP in blood-buffer). All measurements were performed in triplicate.

pH-activity profiles: The pH profiles were determined over a range of pH 2.0-9.0 as described previously (Camarero et al., 2012).

Halide inhibition (I_{50} determination): The inhibitory effect of fluoride, chloride and bromide was measured using two laccase substrates (ABTS and DMP) at their corresponding optimal pH activity values (in 100 mM sodium acetate buffer (pH 4.0) for ABTS and 100 mM sodium tartrate buffer (pH 5.0) for DMP), as well as at physiological pH (in 100 mM sodium phosphate buffer, pH 7.4). Inhibition was determined by the I_{50} value (the halide concentration at which only 50% of the initial laccase activity is retained), as the complexity of the plots complicated

the extraction of the inhibition constant (K_i). The assay mixture contained 2.4 mM ABTS or DMP, halide (concentrations ranging from 0 to 1100 mM) and purified laccase (0.2 and 1.7 nM for ABTS and DMP, respectively). Each data point represents the mean value determined in at least three independent experiments.

Thermostability (T_{50} determination): The thermostability of the different laccase samples was estimated by determining their T_{50} values as reported in a previous work (García-Ruiz et al., 2010).

Spectro-electrochemical studies

Determination of laccase redox potential: The redox titration of yellow laccase mutants was carried out as described previously for the OB-1 parental type (Mate et al., 2012), with some modifications. Briefly, a micro-spectroelectrochemical cell containing a gold capillary electrode was used, with the potential controlled by a three-electrode BAS LC-3E potentiostat (Bioanalytical Systems, West Lafayette, IN, USA) where a Ag|AgCl|KCl electrode was used as reference electrode (BAS) and a platinum wire as counter electrode. The absorbance spectra were monitored on a HR4000 high resolution spectrometer with an effective range of 200-1100 nm using a DH-2000 light source, both from Ocean Optics (Dunedin, FL, USA). The redox potential of the T1 site of the enzyme was determined by mediated redox titration (MRT) using the spectroelectrochemical set-up described above. A complex mediator system was used for the MRT containing three different redox mediators: $K_4[Fe(CN)_6]$ and $K_4[Mo(CN)_8]$ with formal redox potentials of

+430 mV and +780 mV *vs* NHE, respectively, and $K_4[W(CN)_8]$ with a formal redox potential of +520 mV *vs* NHE, synthesized as described previously (Leipoldt et al., 1974). All experiments were performed in 50 mM sodium phosphate buffer pH 7.4.

Electrochemical measurements: Electrochemical experiments were performed with an Autolab PGSTAT30 analyzer controlled by GPES 4.9 software (Eco Chemie, The Netherlands). Experiments were run in a 3-electrode glass cell using a BAS Ag|AgCl|KCl reference electrode (+210 mV *vs* NHE) and a platinum wire counter electrode. The low-density graphite (LDG electrodes) were abraded with sandpaper and sonicated. A 5-μL drop of laccase (13 mg/mL) was deposited on a clean LDG electrode and after it had been absorbed for 20 min, the electrode was set into the electrochemical cell, which was bubbled with O_2 (g) at 1 atm pressure for 15 min. For electrocatalytic measurements, current densities are expressed relative to the geometric area of the electrodes and potentials are described relative to that of the NHE. Cyclic voltammograms were recorded from +1100 mV to +210 mV using a 10-mV/s scan rate.

Protein Modeling

Protein models of the parental and evolved laccases were generated and analyzed as described previously (Maté et al., 2010).

SUPPLEMENTAL INFORMATION

Supplemental information includes five tables, three figures, and Supplemental Results Section.

ACKNOWLEDGEMENTS

We would like to thank Dr. Francisco J. Plou from the ICP (CSIC, Spain) for assistance with the HPLC purification. This study was based upon work funded by EU Projects [NMP4-SL-2009-229255-3D-Nanobiodevice, FP7-KBBE-2010-4-26537-Peroxicats and COST Action CM0701] and a project from the Spanish Government [BIO2010-19697]. D.M.M. was supported by a JAE grant and D.G.P by a Peroxicats contract. M.P. received support from the 2009 Ramón y Cajal programme of the Spanish MINECO.

REFERENCES

Alcalde, M., Ferrer, M., Plou, F.J., and Ballesteros, A. (2006). Environmental biocatalysis: from remediation with enzymes to novel green processes. Trends Biotechnol. *24*, 281-287.

Alcalde, M. (2007). Laccases: biological functions, molecular structure and industrial applications. In Industrial Enzymes: Structure, Function and Applications, J. Polaina & A.P. MacCabe. eds. (Dordrecht, The Netherlands: Springer). pp. 461-476.

Alcalde, M. (2010). Mutagenesis protocols in *Saccharomyces cerevisiae* by *in vivo* overlap extension. In *In vitro* mutagenesis protocols, 3rd ed. Methods in Molecular Biology, 634. J. Braman, ed. (Totowa, NJ: Springer-Humana Press). pp. 3-14.

Borreli, K. W., Vitalis, A., Alcantara, R., and Guallar, V. (2005). PELE: Protein energy landscape exploration. A novel Monte Carlo based technique. J. Chem. Theory Comput. *1*, 1034-1311.

Bullen, R.A., Arnot, T.C., Lakeman, J.B., and Walsh, F.C. (2006). Biofuel cells and their development. Biosens. Bioelectron. *21*, 2015-2045.

Camarero, S., Pardo, I., Cañas, A.I., Molina, P., Record, E., Martinez, A.T., Martinez, M.J., and Alcalde, M. (2012). Engineering platforms for directed evolution of laccase from *Pycnoporus cinnabarinus*. Appl. Environ. Microb. *78*, 1370-1384.

Castillo, J., Gaspar, S., Leth, S., Niculescu, M., Mortari, A., Bontidean, I., Soukharev, V., Dorneanu, S.A., Ryabov, A.D., and Csoregi, E. (2004). Biosensors for life quality - Design, development and applications. Sensor. Actuat. B-Chem. *102*, 179-194.

Christensen, N. J., and Kepp, K. P. (2012). Accurate stabilities of laccase mutants predicted with a modified FoldX protocol. J. Chem. Inf. Model. *52*, 3028-3042.

Couto, S.R. and Herrera, J.L.T. (2006). Industrial and biotechnological applications of laccases: A review. Biotechnol. Adv. *24*, 500-513.

Cusano, A.M., Mekmouche, Y., Meglecz, E., and Tron, T. (2009). Plasticity of laccase generated by homeologous recombination in yeast. FEBS J. *276*, 5471-5480.

García-Ruiz, E., Maté, D., Ballesteros, A., Martinez, A.T., and Alcalde, M. (2010). Evolving thermostability in mutant libraries of ligninolytic oxidoreductases expressed in yeast. Microb. Cell. Fact. *9*, 17.

Garzillo, A.M.V., Colao, M.C., Caruso, C., Caporale, C., Celletti, D., and Buonocore, V. (1998). Laccase from the white-rot fungus *Trametes trogii*. Appl. Microbiol. Biot. *49*, 545-551.

Gianfreda, L., Xu, F., and Bollag, J.M. (1999). Laccases: a useful group of oxidoreductive enzymes. Bioremed. J. *3*, 1-25.

Gonzalez-Perez, D., Garcia-Ruiz, E., and Alcalde, M. (2012). *Saccharomyces cerevisiae* in directed evolution: An efficient tool to improve enzymes. Bioengineered *3*, 172-177.

Guallar, V., and Wallrapp, F. (2008). Mapping protein electron transfer pathways with QM/MM methods. J. R. Soc. Interface *5*, S233-S239.

Jimenez-Juarez, N., Roman-Miranda, R., Baeza, A., Sánchez-Amat, A., Vazquez-Duhalt, R., and Valderrama, B. (2005). Alkali and halide-resistant catalysis by the multipotent oxidase from *Marinomonas mediterranea*. J. Biotechnol. *117*, 73-82.

Kim, J., Jia, H.F., and Wang, P. (2006). Challenges in biocatalysis for enzyme-based biofuel cells. Biotechnol. Adv. *24*, 296-308.

Kittl, R., Mueangtoom, K., Gonaus, C., Khazaneh, S.T., Sygmund, C., Haltrich, D., and Ludwig, R. (2012). A chloride tolerant laccase from the plant pathogen ascomycete *Botrytis aclada* expressed at high levels in *Pichia pastoris*. J. Biotechnol. *157*, 304-314.

Kunamneni, A., Camarero, S., García-Burgos, C., Plou, F.J., Ballesteros, A., and Alcalde, M. (2008). Engineering and applications of fungal laccases for organic synthesis. Microb. Cell Fact. *7*, 1-17.

Leipoldt, J.G., Bok, L.D.C., and Cilliers, P.J. (1974). Preparation of potassium octacyanotungstate (IV) dihydrate. Z. Anorg. Allg. Chem. *407*, 350-352.

Madzak, C., Mimmi, M.C., Caminade, E., Brault, A., Baumberger, S., Briozzo, P., Mougin, C., and Jolivalt, C. (2006). Shifting the optimal pH of activity for a laccase from the fungus *Trametes versicolor* by structure-based mutagenesis. Protein Eng. Des. Sel. *19*, 77-84.

Martínez, A.T., Ruiz-Dueñas, F.J., Martínez, M.J., del Río, J.C., and Gutiérrez, A. (2009). Enzymatic delignification of plant cell wall: from nature to mill. Curr. Opin. Biotech. *20*, 348-357.

Maté, D., García-Burgos, C., García-Ruiz, E., Ballesteros, A.O., Camarero, S., and Alcalde, M. (2010). Laboratory evolution of high-redox potential laccases. Chem. Biol. *17*, 1030-1041.

Maté, D., García-Ruiz, E., Camarero, S., and Alcalde, M. (2011). Directed evolution of fungal laccases. Curr. Genomics *12*, 113-122.

Mate, D.M., Garcia-Ruiz, E., Camarero, S., Shubin, V.V., Falk, M., Shleev, S., and Alcalde, M. (2012). Switching from blue to yellow: Altering the spectral properties of a high redox potential laccase by directed evolution. Biocat. Biotransfor. (in press).

Matera, I., Gullotto, A., Tilli, S., Ferraroni, M., Scozzafava, A., and Briganti, F. (2008). Crystal structure of the blue multicopper oxidase from the white-rot fungus *Trametes trogii* complexed with p-toluate. Inorg. Chim. Acta *361*, 4129-4137.

Morozova, O.V., Shumakovich, G.P., Gorbacheva, M.A., Shleev, S.V., and Yaropolov, A.I. (2007). "Blue" laccases. Biochemistry-Moscow *72*, 1136-1150.

Naki, A., and Varfolomeev, S.D. (1981) Mechanism of the inhibition of laccase activity from *Polyporus versicolor* by halide ions. Biochemistry-Moscow *46*, 1694-1702.

Naqui, A., and Varfolomeev, S.D. (1980) Inhibition mechanism of *Polyporus* laccase by fluoride ion. FEBS Lett. *113*, 157-160.

Niladevi, K.N., Jacob, N., and Prema, P. (2008). Evidence for a halotolerant-alkaline laccase in *Streptomyces psammoticus*: Purification and characterization. Process Biochem. *43*, 654-660.

Riva, S. (2006). Laccases: blue enzymes for green chemistry. Trends Biotechnol. *24*, 219-226.

Rodgers, C.J., Blanford, C.F., Giddens, S.R., Skamnioti, P., Armstrong, F.A., and Gurr, S.J. (2010). Designer laccases: a vogue for high-potential fungal enzymes? Trends Biotechnol. *28*, 63-72.

Shleev, S., and Ruzgas, T. (2008). Transistor-like behavior of a fungal laccase. Angew. Chem. Int. Edit. *47*, 7270-7274.

Singh, G., Bhalla, A., Kaur, P., Capalash, N., and Sharma, P. (2011). Laccase from prokaryotes: A new source for an old enzyme. Rev. Environ. Sci. Biotechnol. *10*, 309-326.

Witayakran, S., and Ragauskas, A.J. (2009). Synthetic applications of laccase in green chemistry. Adv. Synth. Catal. *351*, 1187-1209.

Xu, F. (1996). Oxidation of phenols, anilines, and benzenethiols by fungal laccases: Correlation between activity and redox potentials as well as halide inhibition. Biochemistry *35*, 7608-7614.

Xu, F. (1997). Effects of redox potential and hydroxide inhibition on the pH activity profile of fungal laccases. J. Biol. Chem. *272*, 924-928.

Xu, F., Berka, R.M., Wahleithner, J.A., Nelson, B.A., Shuster, J.R., Brown, S.H., Palmer, A.E., and Solomon, E.I. (1998). Site-directed mutations in fungal laccase: effect on redox potential, activity and pH profile. Biochem. J. *334*, 63-70.

Zhao, H.M., Giver, L., Shao, Z.X., Affholter, J.A., and Arnold, F.H. (1998). Molecular evolution by staggered extension process (StEP) *in vitro* recombination. Nat. Biotechnol. *16*, 258-261.

Zumárraga, M., Camarero, S., Shleev, S., Martínez-Arias, A., Ballesteros, A., Plou, F.J., and Alcalde, M. (2008). Altering the laccase functionality by *in vivo* assembly of mutant libraries with different mutational spectra. Proteins *71*, 250-260.

FIGURE LEGENDS

Figure 1. Directed laccase evolution. The parental type fusion gene (OB-1 mutant) (Maté et al., 2010) is formed by the α-factor prepro-leader, replacing the original laccase signal sequence to improve secretion in *S. cerevisiae*, and the mature laccase. The α-factor pre-leader is represented in orange, the α-factor pro-leader in blue and the mature laccase in red. New mutations are depicted as stars and accumulated mutations as squares; A389- is a deleted residue. TAI (total activity improvement in blood-buffer): a value indicating the improvement in laccase activity detected in *S. cerevisiae* microcultures for each mutant compared with the parental OB-1. Measurements were performed in quintuplicate from supernatants of independent cultures grown in 96-well plates, using 3 mM ABTS (2,2´-azino-bis(3-ethylbenzothiazoline-6-sulfonic acid) as substrate. The $_{ap}I_{50Cl^-}$ (apparent I_{50} for NaCl) indicates the concentration of NaCl at which the enzyme retains 50% of its ABTS-activity, as determined in *S. cerevisiae* microcultures for each mutant after a 2 h incubation. Relative activity at different pH values was assessed with 3 mM ABTS as substrate. Dashed arrows indicate the mutant used as a parent in each generation. N.d., not determined. Silent mutations are not included. Over 10,000 clones were screened in 4 rounds of molecular evolution combining *in vivo* (IvAM, DNA shuffling, IVOE) and *in vitro* (error-prone PCR, mutagenic StEP) recombination/mutagenic methods. In the last cycle of evolution, the final variant (ChU-B) was obtained after analyzing

several positions by site-directed mutagenesis and saturation mutagenesis (**see Supplemental Results Section; see also Table S1**).

Figure 2. Activity in physiological fluids and spectro-electrochemical characterization. (**a**) Activity of the ChU-B mutant determined by measuring O_2 consumption. To monitor laccase activity in blood and plasma, the fluids were supplemented with 10 mM ascorbic acid and the pH adjusted to 7.4 prior to adding the enzyme. (**b**) Redox titration of ChU-B at physiological pH values. Each redox titration was carried out in both directions (*i.e.,* from the fully oxidized to the fully reduced state of the enzyme -reductive titration- and *vice versa* -oxidative titration-). The spectra of laccases were recorded at redox equilibrium and typical spectra of the oxidized, partly reduced and fully reduced enzymes are depicted. Equilibration of the T1 copper center at each potential applied was apparent from the stabilization of absorbance at 600 nm. As the redox mediators used are transparent above 500 nm, the spectral changes at 600 nm were attributed to the T1 Cu of the laccase. Spectra from the reductive titration, corresponding to oxidized laccase (black curve, applied potential +1000 mV *vs* NHE), partly reduced enzymes (red and blue curves, +700 mV and +600 mV *vs* NHE, respectively) and the fully reduced laccase (green curve, +300 mV *vs* NHE) are shown. Insert: a typical Nernst plot of the dependence of the applied potential versus absorbance at 600 nm, and averaged parameters calculated from the reductive and oxidative titrations (mid-point value of +720 mV *vs* NHE and a slope of 110 mV).

(**c**) Cyclic voltammograms of O_2 reduction obtained using a polished, low-density graphite (LDG) electrode (black), and a LDG electrode with ChU-B laccase adsorbed to its surface (red). Measurements were carried out in a three-electrode electrochemical cell filled with 100 mM sodium phosphate buffer pH 7.4 and after bubbling O_2 at a pressure of 1 atm for 15 min, using a platinum wire as the counter electrode and a BAS Ag/AgCl reference electrode. Measurements were performed using Autolab PGSTAT30 controlled by GPES 4.9 software.

Figure 3. Biochemical characterization. White circles, parental type; black circles, ChU-B mutant. pH activities profiles were measured in 100 mM Britton and Robinson buffer at different pH values with 3 mM DMP (**a**) or ABTS (**b**) as substrates. Laccase activity was normalized to the optimum activity value. (**c-e**) Inhibition by halides: (**c**) Cl^- inhibition measured with 2.4 mM ABTS in 100 mM sodium acetate buffer pH 4.0. (**d**) F^- inhibition measured with 2.4 mM ABTS in 100 mM sodium acetate buffer pH 4.0. (**e**) Cl^- inhibition of ChU-B measured with 2.4 mM ABTS in 100 mM sodium phosphate buffer pH 7.4. Each value represents the mean and standard deviation derived from three independent experiments. See also **Figure S1, Tables S2, S3**.

Figure 4 Details of the mutations in the ChU-B variant (**b**) compared with the corresponding residues in the parental type (**a**). The F396I and F454E mutations are shown in yellow, and the I452V mutation (reverted in ChU-B) in black. Blue spheres represent copper atoms. The residues of the internal transfer pathway from T1 Cu to T2/T3 cluster

are colored magenta. Residues involved in the first coordination sphere of the catalytic coppers and their interactions (as green dashes) are also represented. The electrostatic surface of the protein structure is shown in the background. The 3D-structure model is based on the crystal structure of the *Trametes trogii* laccase (97% identity, PDB: 2HRG) (Matera et al., 2008). See also **Figures S2, S3; Table S4**.

Figure1

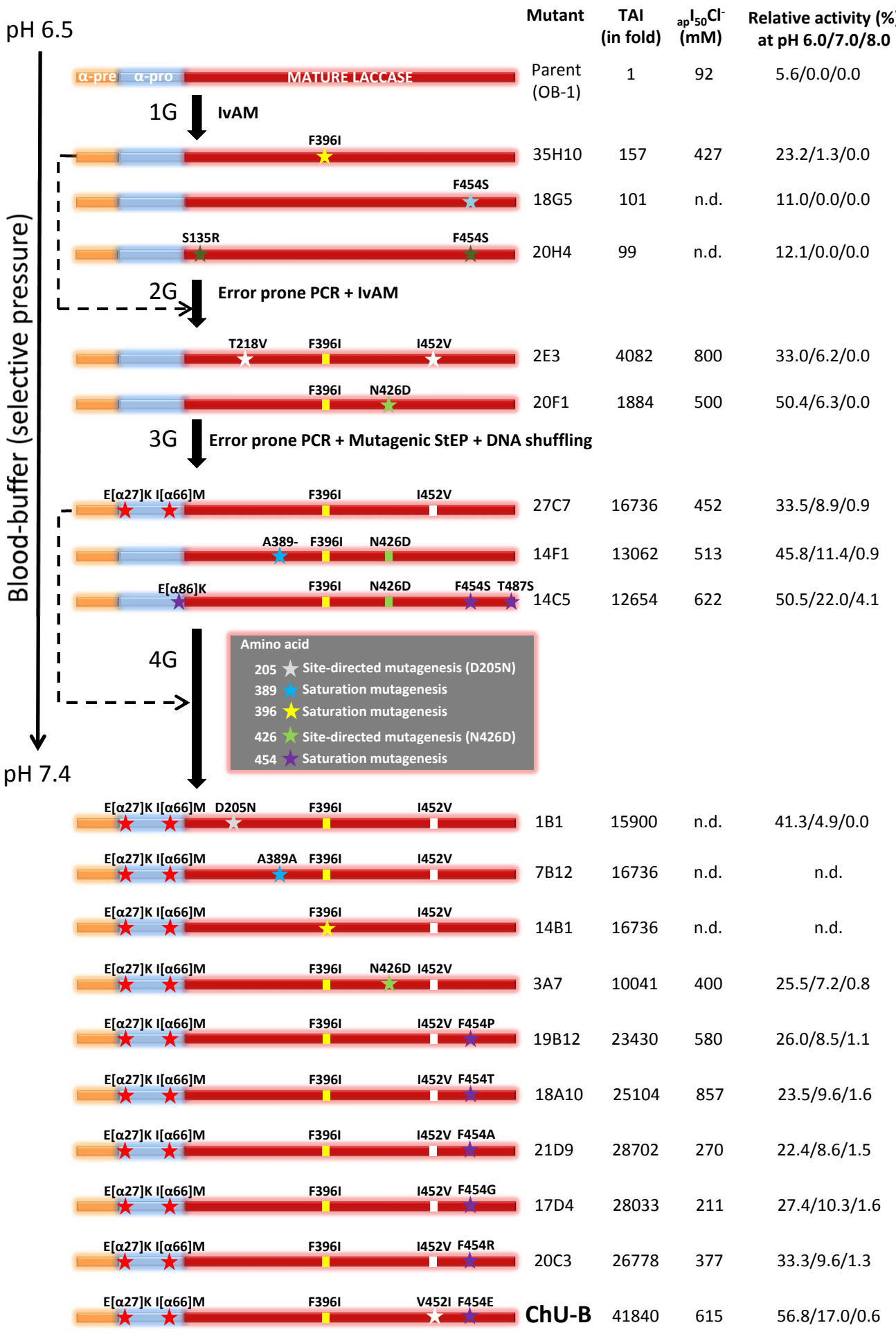

Mutant	TAI (in fold)	$_{ap}I_{50}Cl^-$ (mM)	Relative activity (%) at pH 6.0/7.0/8.0
Parent (OB-1)	1	92	5.6/0.0/0.0
35H10	157	427	23.2/1.3/0.0
18G5	101	n.d.	11.0/0.0/0.0
20H4	99	n.d.	12.1/0.0/0.0
2E3	4082	800	33.0/6.2/0.0
20F1	1884	500	50.4/6.3/0.0
27C7	16736	452	33.5/8.9/0.9
14F1	13062	513	45.8/11.4/0.9
14C5	12654	622	50.5/22.0/4.1
1B1	15900	n.d.	41.3/4.9/0.0
7B12	16736	n.d.	n.d.
14B1	16736	n.d.	n.d.
3A7	10041	400	25.5/7.2/0.8
19B12	23430	580	26.0/8.5/1.1
18A10	25104	857	23.5/9.6/1.6
21D9	28702	270	22.4/8.6/1.5
17D4	28033	211	27.4/10.3/1.6
20C3	26778	377	33.3/9.6/1.3
ChU-B	41840	615	56.8/17.0/0.6

Figure2

a

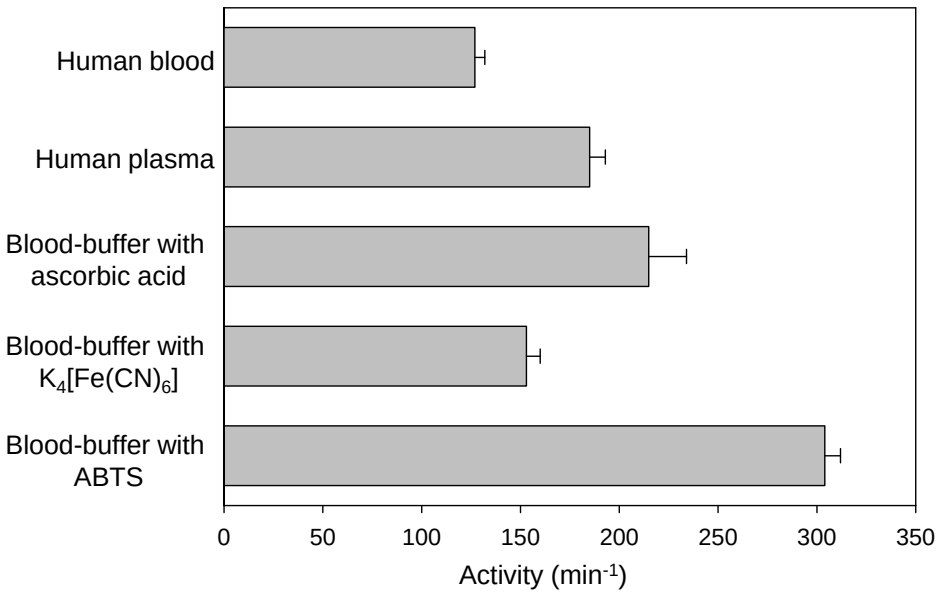
Human blood
Human plasma
Blood-buffer with ascorbic acid
Blood-buffer with $K_4[Fe(CN)_6]$
Blood-buffer with ABTS
0
50
100
150
200
250
300
350
Activity (min^{-1})

b

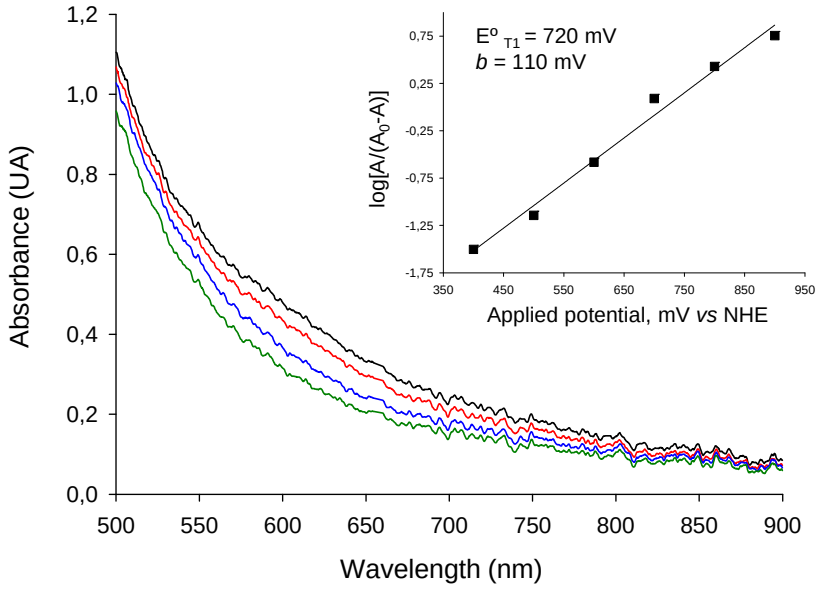
Absorbance (UA)
1,2
1,0
0,8
0,6
0,4
0,2
0,0
500
550
600
650
700
750
800
850
900
Wavelength (nm)
E^o_{T1} = 720 mV
b = 110 mV
log[A/(A0-A)]
0,75
0,25
-0,25
-0,75
-1,25
-1,75
350
450
550
650
750
850
950
Applied potential, mV *vs* NHE

c

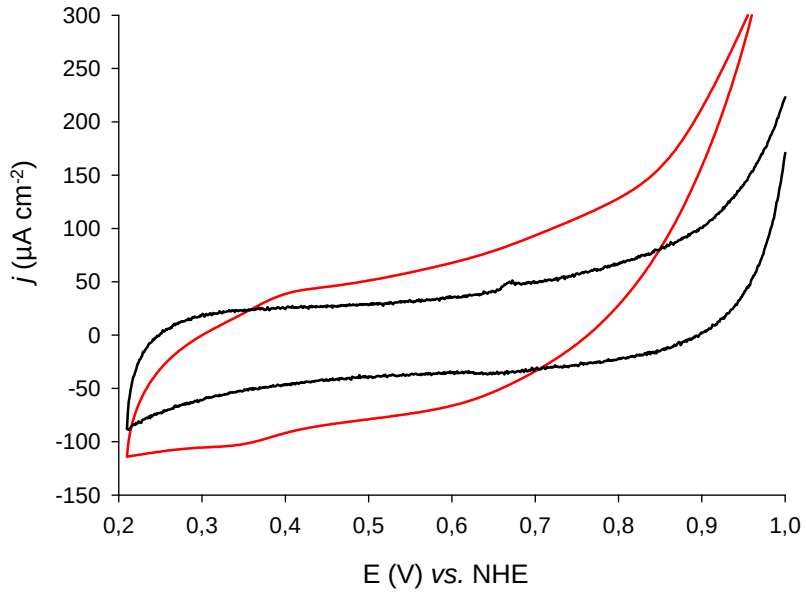
j (µA cm^{-2})
300
250
200
150
100
50
0
-50
-100
-150
0,2
0,3
0,4
0,5
0,6
0,7
0,8
0,9
1,0
E (V) *vs.* NHE

Figure3

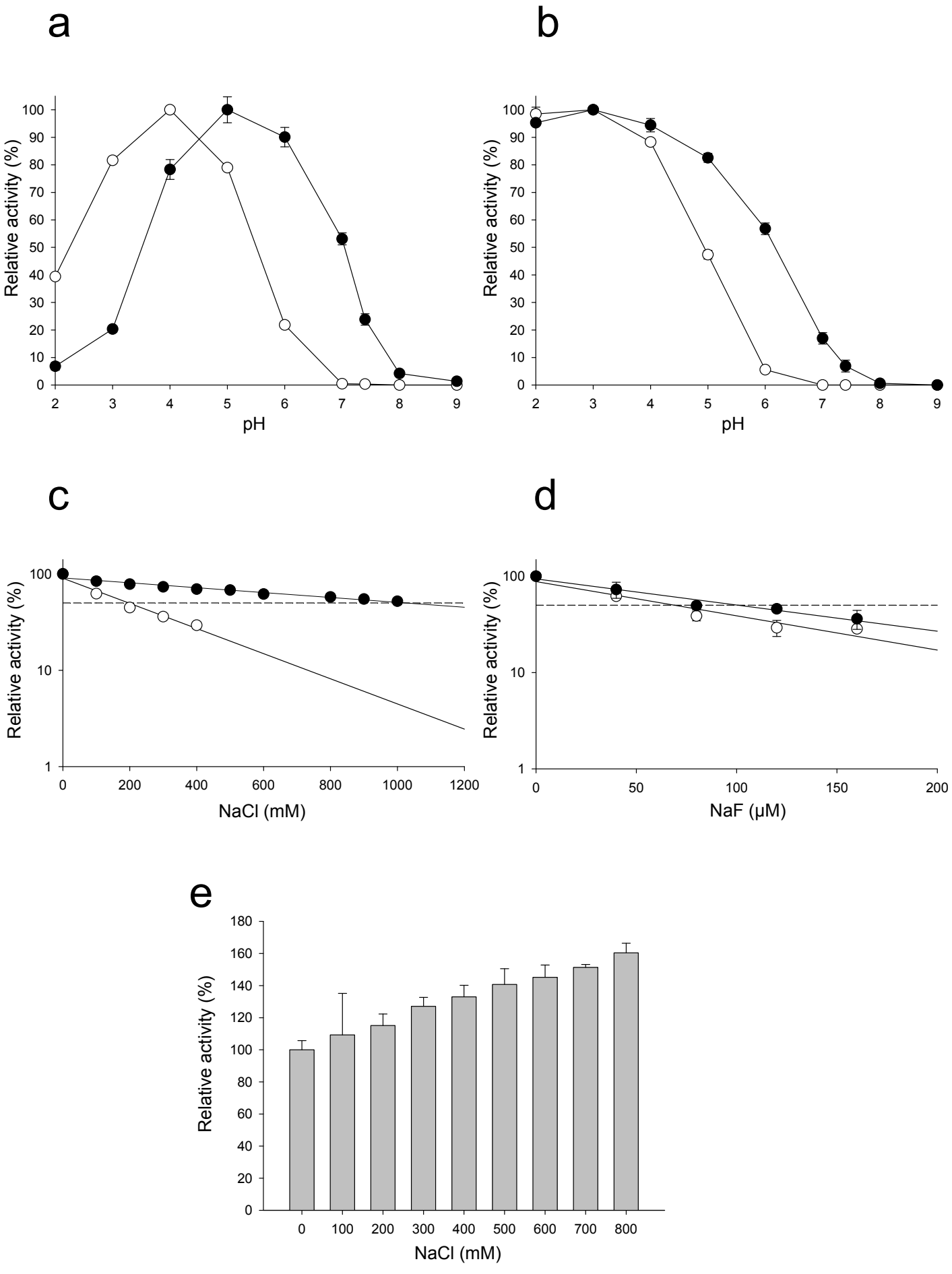

Figure4

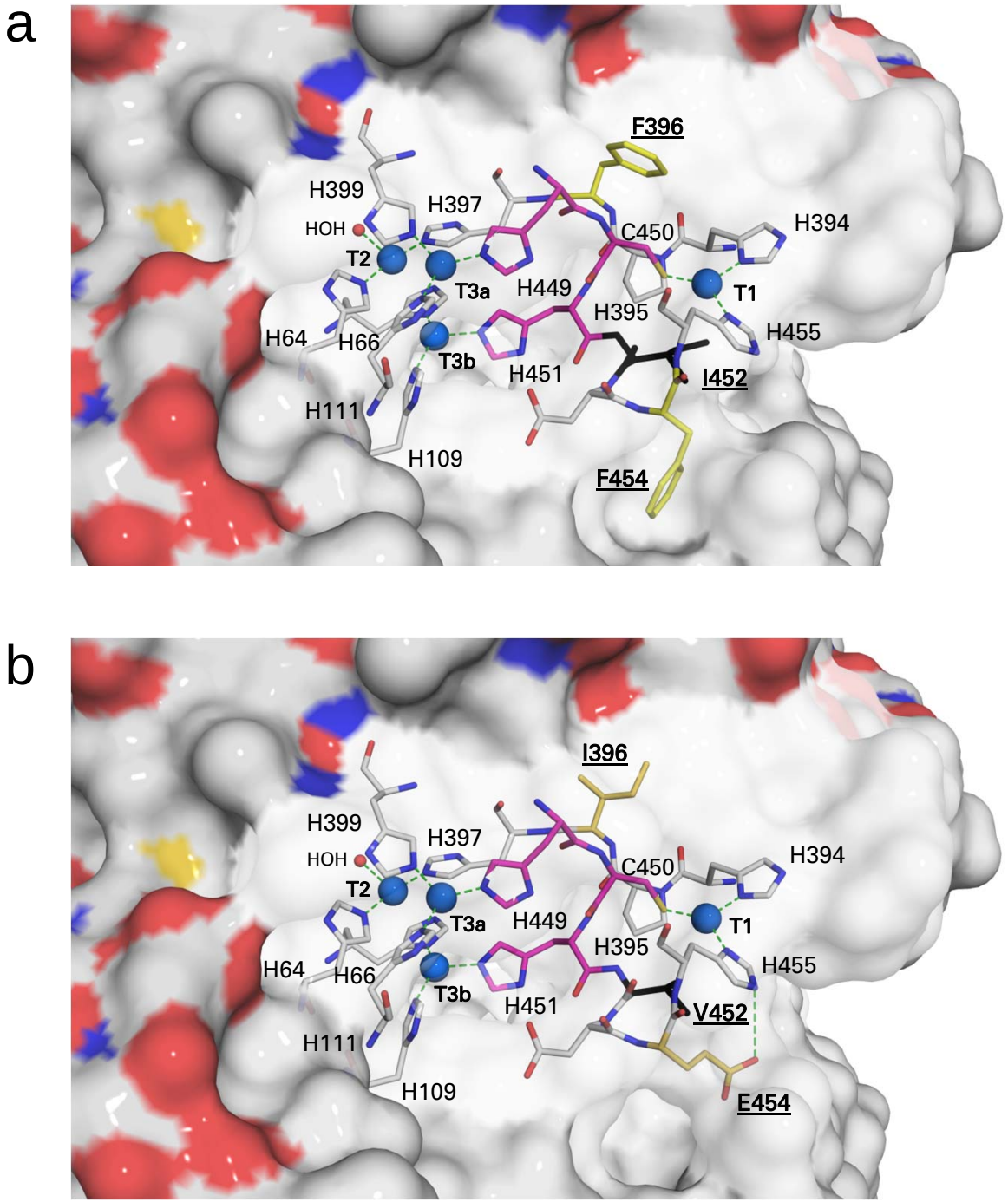
a
F396
H399
H397
HOH
T2
T3a
C450
H394
H449
T1
H395
H64
H66
T3b
H455
H451
I452
H111
H109
F454
b
I396
H399
H397
HOH
T2
T3a
C450
H394
H449
T1
H395
H64
H66
T3b
H455
H451
V452
H111
H109
E454

INVENTORY SUPPLEMENTAL DATA

Table S1: Mutations introduced during the whole laboratory evolution, including nucleotide changes and codon usage for synonymous mutations. Complementary to Figure 1.

Table S2: I50 values for F^-, Cl^- and Br^-. Related to Figure 3.

Table S3: Maximum turnover rates for parent and mutant. Related to Figure 3.

Table S4: Mutations in evolved laccase. Related to Figure 4.

Table S5: primers list.

Fig-S1: pH activity profiles of parental laccase and its mutants. Related to Figure 3.

Fig-S2: Overview of all the residues mutated by evolution. Related to Figure 4.

Fig-S3: Saturation mutagenesis at residue 454. Related to Figure 1.

Additional Results section includes:

Generation four: positions and discussion about residues subjected to site-directed mutagenesis and saturation mutagenesis, specifically: D205N; N426D and saturation mutagenesis at positions 389, 396 and 454.

Supplemental Text and Figures

Fig. S1

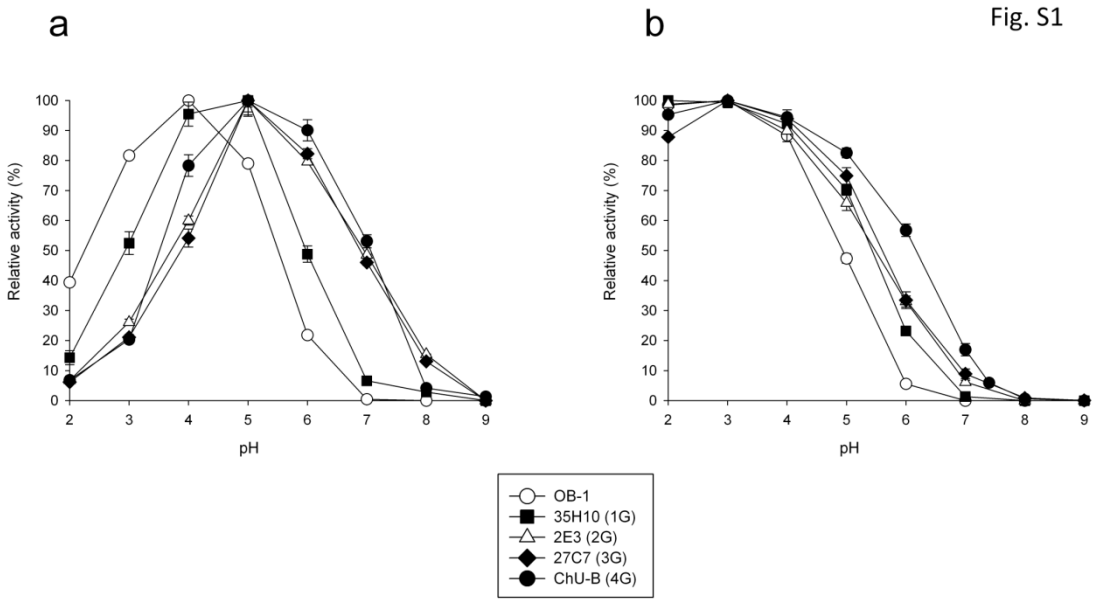

Fig. S2

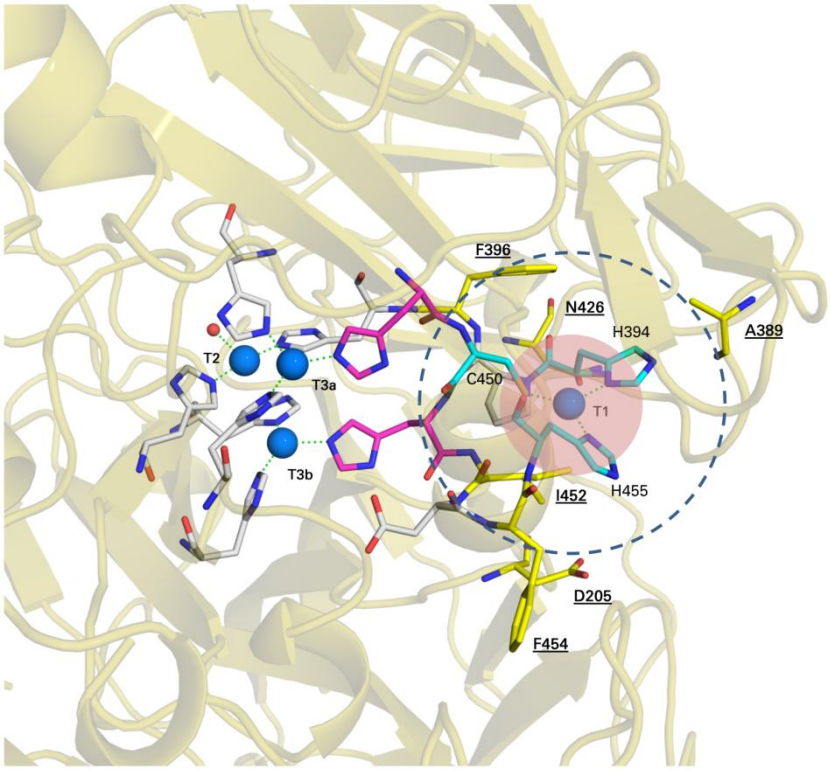

Fig. S3

a

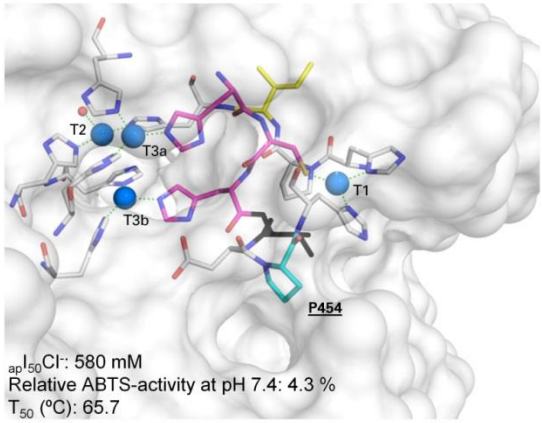

$_{ap}I_{50}Cl^-$: 580 mM
Relative ABTS-activity at pH 7.4: 4.3 %
T_{50} (ºC): 65.7

b

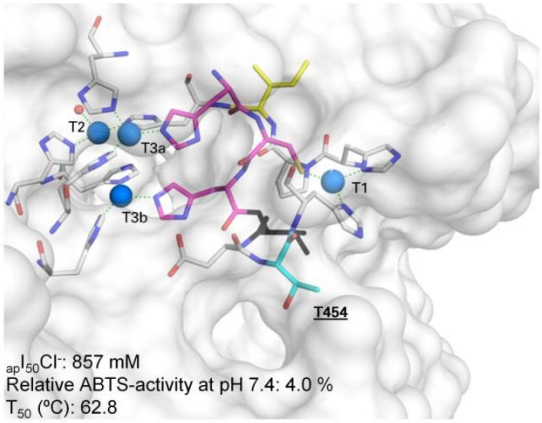

$_{ap}I_{50}Cl^-$: 857 mM
Relative ABTS-activity at pH 7.4: 4.0 %
T_{50} (ºC): 62.8

c

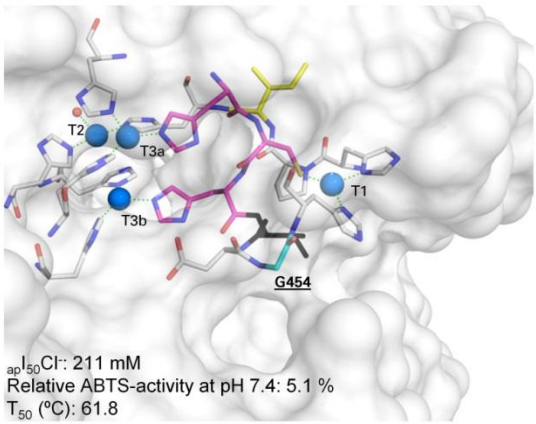

$_{ap}I_{50}Cl^-$: 211 mM
Relative ABTS-activity at pH 7.4: 5.1 %
T_{50} (ºC): 61.8

d

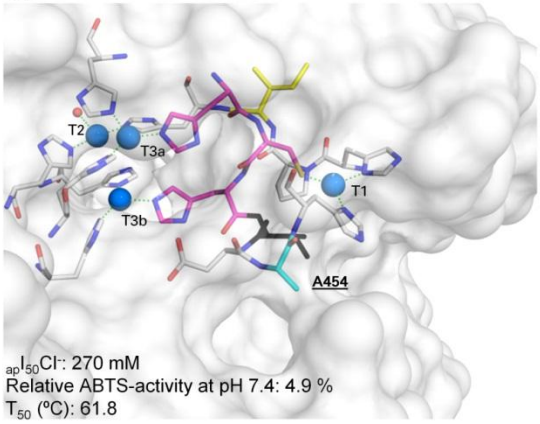

$_{ap}I_{50}Cl^-$: 270 mM
Relative ABTS-activity at pH 7.4: 4.9 %
T_{50} (ºC): 61.8

e

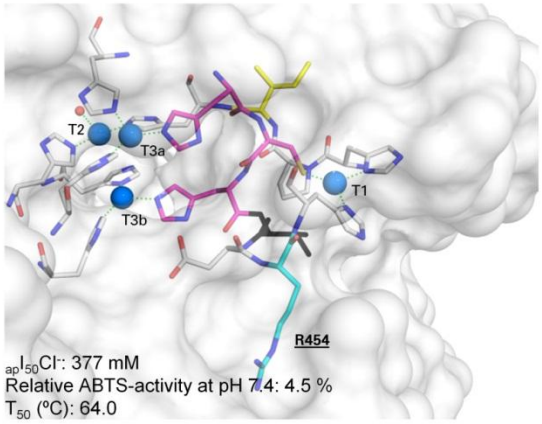

$_{ap}I_{50}Cl^-$: 377 mM
Relative ABTS-activity at pH 7.4: 4.5 %
T_{50} (ºC): 64.0

f

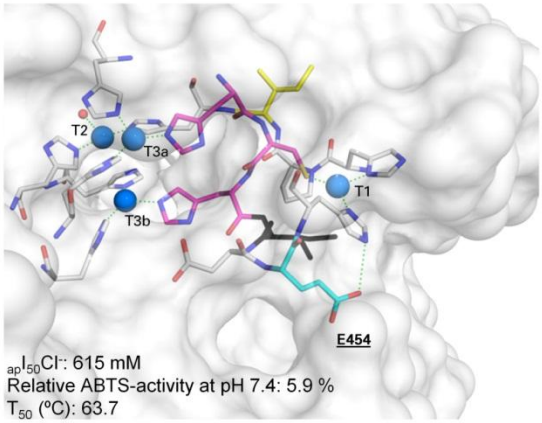

$_{ap}I_{50}Cl^-$: 615 mM
Relative ABTS-activity at pH 7.4: 5.9 %
T_{50} (ºC): 63.7

SUPPLEMENTARY FIGURE LEGENDS

Figure S1. pH activity profiles of the parental laccase and the best mutants of each round of evolution. Activities were measured in 100 mM Britton and Robinson buffer at different pH values with 3 mM DMP (**a**) or ABTS (**b**) as substrates. Laccase activity was normalized to the optimum activity, each value representing the mean and standard deviation derived from three independent experiments. See also Figure 3.

Figure S2. Overview of the mutations in the laccase structure. All the residues mutated in this study are highlighted in yellow. The first coordination sphere of the T1 Cu (His394, His455, Cys450) is indicated with a red circle. Dashed concentric circle indicates the second coordination sphere. The His residues of the internal electron transfer pathway from the T1 Cu to T2/T3 cluster are depicted in magenta. Blue spheres represent copper atoms. The 3D-structure model is based on the crystal structure of the *Trametes trogii* laccase (97% identity) (Matera et al., 2008). See also Figure 4.

Figure S3. Saturation mutagenesis at residue 454 (shown in cyan and underlined): (**a**) 19B12 variant; (**b**) 18A10 variant; (**c**) 17D4 variant; (**d**) 21D9 variant; (**e**) 20C3 variant; (**f**) ChU-B variant. Blue spheres represent copper atoms. The residues of the internal transfer pathway from the T1 Cu to T2/T3 cluster are depicted in magenta. The residues involved in the first coordination sphere of the catalytic coppers and their interactions (green dashes) are also represented. The electrostatic surface of the protein structure is shown in the background. The 3D-structure model is based on the crystal structure of the *Trametes trogii* laccase (97% identity) (Matera et al., 2008). See also Figure 1.

Generation		1G			2G		3G			4G									
Mutation		35H10	18G5	20H4	2E3	20F1	27C7	14F1	14C5	1B1	7B12	14B1	3A7	19B12	18A10	21D9	17D4	20C3	ChU-B
Amino acid	Codon																		
E(α27)K	A**G**A/A**A**A						+			o	o	o	o	o	o	o	o	o	o
D(α49)D	GA**T**$_{38}$/GA**C**$_{20}$	+			o	o	o	o	o	o	o	o	o	o	o	o	o	o	o
I(α66)M	AT**A**/AT**G**						+			o	o	o	o	o	o	o	o	o	o
E(α86)K	**G**AG/**A**AG								+										
S135R	AG**C**/AG**G**			+															
D205N	**G**AC/**A**AC									●									
T218V	A**C**C/A**T**C				+														
D363D	GA**C**$_{20}$/GA**T**$_{38}$		+																
E380E	GA**G**$_{19}$/GA**A**$_{46}$						+			o	o	o	o	o	o	o	o	o	o
A389-	GCC/---							+											
A389A	GC**C**$_{13}$/GC**G**$_{6}$										■								
F396I	**T**TC/**A**TC	+			o	o	o	o	o	o	o	■	o	o	o	o	o	o	o
F403F	TT**C**$_{18}$/TT**T**$_{26}$		+																
T413T	AC**G**$_{8}$/AC**A**$_{18}$						+			o	o	o	o	o	o	o	o	o	o
N426D	**A**AC/**G**AC					+		o	o				●						
I452V	**A**TC/**G**TC				+		o			o	o	o	o	o	o	o	o	o	□
F454S	T**T**C/T**C**C		+	+					+										
F454P	**TT**C/**CC**C													■					
F454T	**TTC**/**ACG**														■				
F454A	**TTC**/**GCG**															■			
F454G	**TT**C/**GG**C																■		
F454R	**TTC**/**CGG**																	■	
F454E	**TTC**/**GAG**																		■
A458A	GC**T**$_{21}$/GC**C**$_{13}$								+										
F460F	TT**C**$_{18}$/TT**T**$_{26}$								+										
T487S	A**C**C/A**G**C								+										
TAI (in fold) mutant/OB-1 (parent)		157	101	99	4082	1884	16736	13062	12654	15900	16736	16736	10041	23430	25104	28702	28033	26778	41840
Apparent I_{50} NaCl (mM)		427	n.d.	n.d.	800	500	452	513	622	n.d.	n.d.	n.d.	400	580	857	270	211	377	615
Relative activity (%) at pH 7.0		1.3	0.0	0.0	6.2	6.3	8.9	11.4	22.0	4.9	n.d.	n.d.	7.2	8.5	9.6	8.6	10.3	9.6	17.0
T_{50} (°C)		69.5	68.1	65.1	68.0	69.0	68.5	66.8	60.0	n.d.	n.d.	n.d.	68.9	65.7	62.8	61.8	61.8	64.0	63.7

Supplementary Table S1. Mutations introduced during the directed evolution process. +, new mutation; o, accumulated mutation; ●, mutation introduced by site-directed mutagenesis; ■, mutation introduced by saturation mutagenesis; □, reverted mutation (V452I, **G**TC/**A**TC). Silent mutations are underlined; subscript indicates codon usage in *S. cerevisiae*. TAI, total activity improvement in blood-buffer. See also Figure 1.

Supplementary Table S2. Parental and ChU-B mutant I_{50} values (in mM) for different halides. [a]Experiments were carried out at the optimum pH value for each substrate. [b]n.m., non measurable. See also Figure 3.

Inhibitor	Substrate	pH[a]	OB-1 mutant	ChU-B mutant
NaF	ABTS	4.0	0.070	0.109
	DMP	5.0	0.167	0.183
NaCl	ABTS	4.0	176	1025
	DMP	5.0	208	818
NaBr	DMP	4.0	1306	n.m.[b]

Supplementary Table S3. Maximum turnover rates (mol substrate/min/mol enzyme) for the parental laccase and ChU-B mutant under optimum conditions and in blood buffer. [a]Optimum pH activity value (4.0 and 5.0 for parent and ChU-B, respectively). n.m., non measurable. See also Figure 3.

Substrate	pH	Parent type	ChU-B mutant
ABTS	3.0	44215 ± 1061	14895 ± 654
	7.4 (blood buffer)	n.m.	143 ± 9
DMP	Optimum[a]	20820 ± 710	4767 ± 216
	7.4 (blood buffer)	n.m.	427 ± 32

Supplementary Table S4. Mutations introduced into the mature laccase during the directed evolution process. [a]Mutations present in the final ChU-B variant. See also Figure 4.

Mutation	Distance to T1 Cu (Å)	Distance to T2 Cu (Å)	Distance to T3a-T3b Cu (Å)	Domain	Secondary structure motif
I452V	4.8	12.4	9.6	III	Loop (H451-I452)
F454E[a]	7.6	15.8	12.2	III	α-helix (D453-A458)
F396I[a]	7.6	9.9	9.0	III	β-sheet (P395-L398)
A389-	7.7	21.4	18.4	III	Loop (L383-H394)
N426D	9.3	14.5	13.7	III	β-sheet (V424-N426)
D205N	7.8	15.2	11.8	II	Loop (L202-N207)

Supplementary Table S5. Primers employed in this project. The codons subjected to mutagenesis are highlighted in bold, where N is A/T/G/C and S is G/C.

Oligonucleotide	Sequence	Annealing site (bp) in pJRoC30
RMLN forward	5'-CCTCTATACTTTAACGTCAAGG-3'	5'-420-441-3'
RMLC reverse	5'-GGGAGGGCGTGAATGTAAGC-3'	5'-2288-2307-3'
D205N forward	5´-CTGGTGTCGCTGTCATGC**AAC**CCGAATTACACGTTCAGC-3´	5´-1337-1375-3´
D205N reverse	5´-GCTGAACGTGTAATTCGG**GTT**GCATGACAGCGACACCAG-3´	5´-1337-1375-3´
N426D forward	5´-GTCTACCGCGACGTCGTC**GAC**ACGGGCTCGCCCGGGGAC-3´	5´-2000-2038-3´
N426D reverse	5´-GTCCCCGGGCGAGCCCGT**GTC**GACGACGTCGCGGTAGAC-3´	5´-2000-2038-3´
SAT389 forward	5'-CTCCCCGCCACCTCCGCC**NNS**CCCGGCTTCCCGCAC-3'	5'-1889-1924-3'
SAT389 reverse	5'-GTGCGGGAAGCCGGG**SNN**GGCGGAGGTGGCGGGGAG-3'	5'-1889-1924-3'
SAT396 forward	5'-CCCGGCTTCCCGCACCCC**NNS**CACTTGCACGGGCACACC-3'	5'-1910-1948-3'
SAT396 reverse	5'-GGTGTGCCCGTGCAAGTG**SNN**GGGGTGCGGGAAGCCGGG-3'	5'-1910-1948-3'
SAT454 forward	5'-CTCCACTGCCACGTCGAC**NNS**CACCTTGAGGCTGGGTTC-3'	5'-2084-2122-3'
SAT454 reverse	5'-GAACCCAGCCTCAAGGTG**SNN**GTCGACGTGGCAGTGGAG-3'	5'-2084-2122-3'

SUPPLEMENTARY RESULTS

In the generation 4, the following positions were subjected to site-directed mutagenesis and saturation mutagenesis (see also **Figure 1, Table S1**).

D205N: this mutation reportedly provokes a shift in the optimum pH value of the *Trametes versicolor* laccase (a 1.4 unit increase with DMP -2,6-dimethoxyphenol- as the substrate) (Madzak et al., 2006). The same substitution was tested in this study, giving rise to the 1B1 mutant, which resulted in a comparable improvement (2.0 unit increase over the parental type with DMP as the substrate). 1B1 was finally excluded due to its low TAI value and activity with non-phenolic compounds at physiological pH values.

N426D: this beneficial mutation was first discovered in the 20F1 mutant (2G) but it was eventually lost because of the low likelihood of a crossover event with the nearby I452V. N426D was introduced in 27C7 to create the 3A7 variant, resulting in a 0.6-fold decrease in activity.

Saturation mutagenesis at positions 389, 396 and 454: the Ala389 residue was deleted in the third round of evolution, enhancing the TAI ~3-fold compared to the best performing parent in the previous generation (2E3 mutant). After saturation mutagenesis and screening, only A389A mutants were discovered, indicating that unless the whole residue is removed, no other amino acid is better suited at this position. Phe396 was subjected to saturation mutagenesis because the F396I mutation conferred the greatest improvement in the entire evolution experiment (a 157-fold improvement in the 35H10 mutant, 1G). Besides, this mutation changed by itself the pH profile for DMP as substrate (from 4.0 to 5.0) without jeopardizing the thermal stability (**Fig. S1**). After saturation mutagenesis and screening, all variants